Lithium Niobate Dispersed Silver Sulphate – A Composite Solid Electrolyte

S. W. Anwane
Department of Physics, Shri Shivaji Science College, Congress Nagar, Nagpur, India 440012
Tel: (+91) 7122423432;Fax:(+91)7122440955
E-mail:swanwane2000@yahoo.com

Abstract:
Composite materials which are heterogeneous mixtures of two or more solid phases offer value added properties over the basic ingredients. This has generated interest for device applications. When silver sulphate possessing moderate silver ion conducting features when dispersed with insulating lithium neobate particles, enhanced electrical conductivity, reduced activation enthalpy of ion migration. Moreover, improved surface morphology is observed due to dispersion of lithium neobate. In the present work, detailed electrical properties have been studied from the Complex Impedance Spectroscopy. Arrhenius Plot, Concentration and Temperature dependent conductivity and activation energy have also been studied. The ionic transference number of the composite system remains unchanged on dispersion thereby retaining its category as Solid Ionic Conductor (SIC). Moreover optimum composition, 30 Wt% $LiNbO_3$ dispersed in $Ag_2SO_4$is the promising material found out of present study that may be further explored for device applications.

Keywords : *lithiumneobate, silver sulphate, fast ionic conductors, solid electrolyte, composites*

Introduction:

Composite materials are heterogeneous mixtures of solid phases. The elaboration of composites offers a new degree of freedom in the search for advanced functional materials, because specific properties can to a certain degree be tailored by mixing appropriate phases. In the domain of solid state ionics, two routes can lead to improved solid ionic conductors: a search for new compounds and structures sustaining high levels of ionic conductivity or a modification of existing compounds, by heterogeneous or homogeneous doping. The latter involves homogenous dissolution of a certain amount of aliovalent dopant in the bulk of the ionic conductor M^+X^- in order to increase the concentration of mobile charge carriers according to bulk defect equilibrium. One example is the creation of additional vacancies by doping with cations of higher valence, such as D^{2+} in substitution of M^+, written in KroÈger-Vink nomenclature **[i]**:

$$DX_2 + 2M_M \rightarrow D_M^{\cdot} + V_M^{'} + 2MX \quad \text{.....(1)}$$

Heterogeneous doping, in contrary, involves mixing with a second phase with very limited solid solubility and the formation of defect concentration profiles in the proximity of interfaces. The deviations from local electrical neutrality (space charges) are a consequence of point defect equilibrium at interfaces **[ii]**. Apart from the improvement of the electrical properties, such as high conductivity and ionic transference number, the development of composite materials can also lead to better mechanical properties, such as better shock resistance or higher strength. Although composite materials can in principle contain many different phases, literature in the field of solid state ionics deals primarily with two-phase mixtures. In 1973, Liang **[iii]** observed an enhancement of ionic conductivity by a factor of almost 50 in a composite material made from lithium iodide LiI, a compound with moderate Liion conductivity at ambient temperature, and dispersed small aluminaAl_2O_3 particles. The maximum lay around 40 vol% alumina. After this initial study, the conductivity enhancement in heterogeneous materials was confirmed for numerous ceramic composites, including

dispersions of fine insulator particles in an ionic conductor matrix and mixtures of two different ionic conductors, with a major contribution by J. B.Wagner [**iv**] and his group. The majority of studies was made on monovalent cation conductors, such as lithium, silver and copper halides, the largest group being lithium compounds, given their importance in high-energy density portable batteries. Besides Al_2O_3, other oxides, such as MgO, SiO_2, CeO_2, $TiO_2$and ferroelectric $BaTiO_3$, were found to be effective second phases for ionic conductivity improvements.

More recently, the composite effect was also observed in ceramic anion conductors, such as lead or calcium fluoride, and even in inorganic solids with trivalent cation conductivity, like aluminum and rare-earths. The theory of ionic conductor composites, whichis developed in the first part, highlights the importance of phase boundaries for the electrical properties. Boundaries can be transport pathways or transport barriers, given their modified core structure (core effects), and can affect the charge carrier distribution in the adjacent regions (space charge effects). Local deviations from electrical neutrality in the vicinity of interfaces were recognized long time ago in the electro-chemistry of liquid electrolytes or in colloidal systems. Gouy [**v**] established the theory of the electrical double layer at the electrode-electrolyte interface in1903 and Overbeek and co-workers [**vi**] the electrostatic colloid theory in 1948. Lehovec [**vii**] calculated in 1953 the defect distribution at the surface of ionic crystals and discussed the implications for ionic conduction. In 1972, Wagner [**viii**] used the space charge layer concept to explain conductivity effects in two-phase materials with electronic conduction, such as metallic inclusions in a semiconducting oxide or mixtures of two semiconducting oxides. After an attempt by Jow and Wagner in 1979 [**ix**], Maier [**x,xi**] established the space charge layer theory of heterogeneous ionic conductors after 1984.In the second part, we present important investigations of ionic conductor composites since Liang's initial study 25 years ago. Ceramic composites, which are mixtures of two crystalline inorganic phases, represent so far the most important group in solid state ionics, but a growing amount of work was recently devoted to glass-ceramic composites, obtained by partial crystallization of a glassy matrix, and polymer-ceramic composites, where an inorganic compound is dispersed in a polymer matrix. Agrawal and Gupta[**xii**] reviewed composite solid electrolytes and gave an extensive list of systems reported in the literature.

Silver sulphate, a non-alkali metal sulphate, is an exception which shows high cationic conductivity in spite of the bigger size of Ag^+. It undergoes a structural phase transition from the high temperature highly conducting hexagonal α-phase to the low temperature moderately conducting orthorhombic β-phase at 416^{o}C. It attracted scant attention until its potential application in SO_x(x=2, 3) galvanic sensors was proved [**xiii**]. Recently, ever since the concept of using a metal/metal sulphate reference electrode in solid electrochemical gas sensors has evolved, it has attracted a great deal of attention. It exhibits many advantages over other sulphate-based [**xiv**] solid electrolytes in engineering SO_2 gas sensors like: (*i*) coexistence of Ag–O–S phase in Ag/Ag_2SO_4; (*ii*) equilibration of antagonist SO_4^{2-}(solid) with SO_2/SO_3 (gas); (*iii*) invariance of high ionic conductivity over the SO_x environment, etc. [**xv,xvi,xvii,xviii,xix,xx,xxi,xxii,xxiii**]

Theory of Ionic Conduction in Composites

Interfaces play an important role for the transport properties of polycrystalline and poly-phase (composite) materials. Given the anisotropy of boundaries, one has to distinguish between transport along and across interfaces. Enhanced ionic conduction along interfaces can be observed for two reasons. First, the interface core itself is a disordered region, where defect formation and migration energies are generally notably reduced. This leads to enhanced ionic transport within the interface core (grain boundary diffusion). However, core effects are generally small, given the reduced interface area in conventional microcrystalline materials. Some studies established the role of grain boundary diffusion in polycrystalline oxides, including NiO, Al_2O_3, MgO [**xxiv**] or ZnO [**xxv**], but there seems to be no similar study in composite materials. Second, point defect and dopant interactions with interfaces, for example accumulation in the interface core (intrinsic and extrinsic interfacial segregation),induce concentration profiles of point defects in the regions adjacent to the interface in ionic materials(space charge layers). Only few quantitative studies exist on grain boundary segregation in oxides, including CaO-doped ZrO_2 [**xxvi**], TiO_2 [**xxvii**] and CeO_2 [**xxviii**], and similar studies on phase boundaries in composite materials are even more difficult, from an experimental as well as a theoretical point of view. The concentration profiles of mobile charge carriers near interfaces are a consequence of thermodynamic defect equilibrium.

Experimental:

The initial ingredients Ag_2SO_4, $LiNbO_3$ where with assay 99.99% were procured from Aldrich Chemicals (USA). These pre - dried initial ingredients with weight fractions (100–x) Ag_2SO_4: (x)$LiNbO_3$ (where x=0–50 weight%), were mixed in an agate mortar under acetone for 2 hrs so as to ensure homogenous mixing. This mixture was latter heated up to the melting point of the host matrix. This ensures the fusing of $LiNbO_3$ in to the molten state of host Ag_2SO_4 and subsequently cooled to room temperature. The ingots, obtained were pulverized to get a fine powder. The powder of each composition was pressed uni-axially using Specac make stainless steel die-punch at pressure of 3 tons/cm^2 to obtain pellet of dimension 9mm in diameter and 1-2 mm thick. Finally the pellets were sintered at 500^{o}C, well below the melting point of host matrix for fixed duration of an hour followed by slow cooling to room temperature.

The prepared samples were characterized by X-ray powder diffraction (XRD) (Philips PW1700 diffractometer attached with PW 1710 controlling unit) using CuK_α radiation. The solid–solid phase transition temperature and the heat of transition were studied by Differential Scanning Calorimetric (DSC) using Mettler TA 4000, DSC 25 at a heating rate of 10^{o}C/min. The microstructures were examined with the help of Scanning Electron Microscope (SEM) (Cambridge 250 Mark-III stereoscan electron microscope). Using Infra Red (IR) spectroscopy, the stack plots of the samples were recorded in several spectral regions of interest using a Perkin-Elmer 983 IR spectrometer.

For electrical characterization, the specimens obtained in the form of circular discs of 9mm diameter and 2mm thickness by pressing the powder with the help of a Specac (UK) stainless steel die-punch and hydraulic press. Prior to spring loading of the pellets between silver electrodes, a good ohmic contact was ensured by using a quality silver paint on both opposite parallel surfaces of the pellet, followed by baking at 200^{o}C for 2 hrs. Preceding the impedance measurement, the spring-loaded sample was heated to 510^{o}C for an hour to homogenize the charge carriers in the sample and simultaneously to remove the moisture

content therein. Later, the temperature of the furnace was reduced in step of 20°C at a cooling rate of 2°C/min. At the end of each cycle the sample was allowed to attain thermal equilibrium for a dwell time of 30 minutes using a Eurotherm 810 PID temperature controller. At the end of each dwell time, the real and imaginary parts of the impedance were measured as parametric functions of frequency in the range 5Hz–13MHz and temperatures from 510 to 100°C during the cooling cycle using an HP 4192A IF impedance analyzer. The entire measurement system was properly shielded to avoid external electrical pickups. A stainless steel faraday cage was employed for this purpose.

The ionic transference number of the specimens was measured by Wagner's dc polarization method using a Keithley SMU 236 with cell configuration:

Ag/Electrolyte/Pt.

A small dc potential was applied across the above configuration to record current at zero and saturation time to know the current under polarized and un-polarized current to obtain the ionic transference number.

$$t_i = \frac{\sigma_0 - \sigma_\infty}{\sigma_0} \qquad \ldots(2)$$

The reproducibility of the impedance data and transference number was confirmed by repeating the measurement on freshly prepared samples.

Result &discussion:

Structural characterization forms the very basis for understanding the structure correlated conduction mechanism.[**xxix,xxx,xxxi,xxxii,xxxiii,xxxiv,xxxv**]

X-ray powder diffraction

The XRD pattern for all six systems (1-*x*) Ag_2SO_4: (*x*) $LiNbO_3$ for x=0, 10, 20, 30, 40, 50 were obtained at room temperature. A comparison of this data with the JCPDS, in the table given below suggests the presence of potential lines corresponding to standard lines corresponding only to Ag_2SO_4 and $LiNbO_3$. Insubstantial variation in *d* values indicates that the second dispersed $LiNbO_3$ phase is insoluble. Moreover, the absence of any new lines rules out a chemical reaction of $Ag_2SO_4$with $LiNbO_3$. A comparison of experimental, *d*, and relative intensity values, I/I_0, with those of JCPDS data is given in **Table 1**for a couple of samples.

Table 1: A comparison of experimental *d* and I/I_0 values with JCPDS data for (1-*x*) Ag_2SO_4: (*x*) $LiNbO_3$ for x=0, 10, 20,

x=0		*x*=10		*x*=20		JCPDS data		
d	I/I_o	d	I/I_o	D	I/I_o	d	I/I_o	Plane, Phases
4.691	11	4.6929	4	--	--	4.699	10	[111]β-Ag_2SO_4
3.993	22	3.9915	11	3.993	32	3.994	25	[220]β- Ag_2SO_4
3.177	71	3.1739	100	3.1738	71	3.177	70	[040]β- Ag_2SO_4
2.873	100	2.8781	20	2.872	38	2.873	100	[311]β- Ag_2SO_4
2.855	10	2.855	10	2.852	11	2.85	100	[110]$LiNbO_3$
2.644	90	2.6436	21	--	--	2.644	90	[022]β- Ag_2SO_4
2.421	33	2.4146	7	2.4633	46	2.421	30	[311]β- Ag_2SO_4
2.314	5	2.314	5	2.3144	31	2.328	30	[111]$LiNbO_3$
1.982	10	1.999	6	2.001	12	1.98	11	[242]β- Ag_2SO_4
-	-	-	-	2.0018	15	2.016	35	[200]$LiNbO_3$

Differential Scanning Calorimetry (DSC)

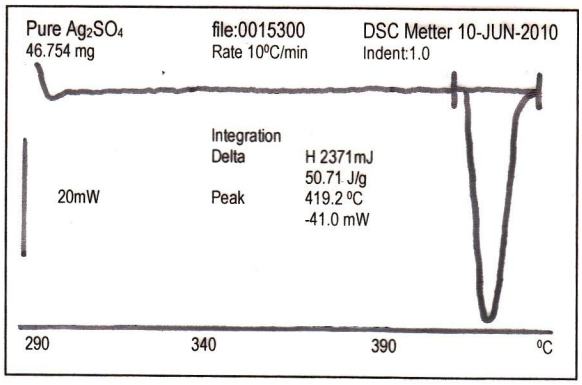

Fig.1: DSC isotherm for pure Ag_2SO_4

Differential Scanning Calorimetric (DSC) studies were carried out on all samples. It was observed that for x=0, 10, 20, 30, 40 weight % the DSC isotherms indicates fall in enthalpy with concentration of $LiNbO_3$. However, transition temperature remains almost invariant. A DSC isotherm for the sample x=0 are depicted in **Fig.1**. The phase transition temperature and heat of transition obtained from the thermograms has been presented in **Table 2**.

Table 2: DSC Data for $(100\text{-}x)Ag_2SO_4$:(x)$LiNbO_3$

Composition	J/gm	T °C
x=0	50.7	429.2
x =10	45.2	429.4
x =20	39.3	430.5
x =30	34.7	429.4
x =40	29.6	429.5

Scanning Electron Microscopy (SEM)

The surface morphology of the $LiNbO_3$dispersed Ag_2SO_4 has been studied using Scanning Electron Microscopy (SEM).

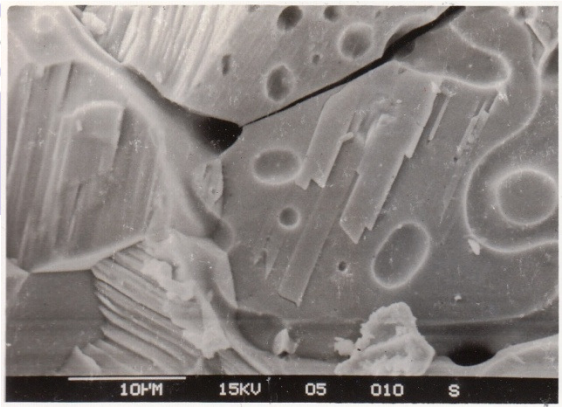

Fig.2: SEM microphotograph of pure Ag_2SO_4

Fig.2 representing microphotograph of pure Ag_2SO_4:$LiNbO_3$. It reveals the polycrystalline grain morphology of the host material obtained at room temperature.

Ionic Transference Number:

The ionic transference number for x=0 to x=40 was carried out using Wagner's DC polarization method using Eq (2) has been presented in **Table 2**.

Table 3: DSC Data for $(100\text{-}x)Ag_2SO_4:(x)LiNbO_3$

Composition	t_i
x=0	0.999
x =10	0.999
x =20	0.999
x =30	0.998
x =40	0.998

The data shows that the ionic contribution to the conductivity of entire compositions does not depend upon the dispersion concentration of $LiNbO_3$ up to 40 wt%.

Impedance Spectroscopy:

The results of complex impedance spectroscopy are critically analyzed to find bulk properties by eliminating extraneous parameters such as electrode polarization and grain boundary. A distorted semicircular arc is observed for the pure sample (**Fig. 3**). A closer look at this figure reveals that the distorted semicircular arc is a combination of two overlapping depressed semicircular arcs. However, there are two discernible semicircular arcs in the case of the rest of the samples.

Since the conductive silver coating on both the surfaces of the electrolyte acts as a reversible (non-blocking) electrode, no electrode polarization is reflected in the complex impedance plane. A non-linear least squares (NLS) fit method is used to ascertain the presence of two overlapping depressed semicircular arcs. In order to accomplish this, the complex impedance data acquired at a fixed temperature using a computer controlled HP 4192A IF impedance analyzer is fitted to the following equation using our software developed in *Turbo C*.

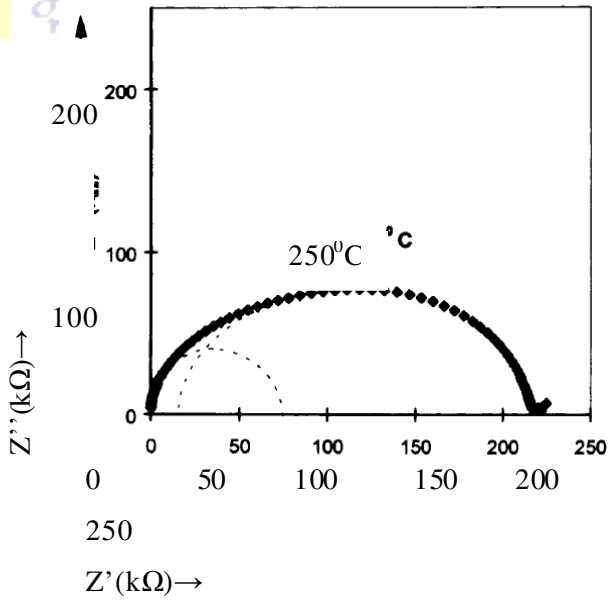

Fig.3: Complex impedance plot for pure Ag_2SO_4 at 250 °C (the doted line represents the best fit curve)

$$Z = Z(0) + \frac{Z(\infty) - Z(0)}{1 + (j\omega\tau)^{\alpha}} \qquad \ldots(3)$$

where $Z(0)$ and $Z(\infty)$ are limiting values of $Z(\omega)$ when ω varies from minimum to maximum, τ is relaxation time, α is empirical measure of departure from ideal Debye model. During the NLS fitting the sum of squares is minimized by unity weighting represented by

$$S_i = (\Delta R_i)^2 + (\Delta I_i)^2 \qquad \ldots(4)$$

whereΔR_i and ΔI_i are the real and imaginary fitting residuals. The presence of two overlapping depressed semicircular arcs is suggestive of the occurrence of two prominent conduction mechanisms simultaneously under the external perturbation ac signal. Various interpretations can be made in the impedance analysis in a polycrystalline ion conducting specimen; however, an experimental impedance obviously contains major contributions from inter-grain and intra-grain ion migration[**xxxvi,xxxvii**]. In order to have a more meaningful discussion, the voluminous impedance data obtained by following the above procedure are fitted in using the equation

$$f_p = f_0 e^{\frac{-Em}{kT}} \qquad \ldots(5)$$

The peak frequency of the complex impedance $\omega_{max} = 2\pi f_p$

$$\frac{1}{\tau} = \frac{1}{RC} = \frac{\sigma}{\varepsilon\alpha\mu C}, \mu = \mu_0 e^{\frac{-Em}{kT}} \qquad \ldots(6)$$

where$\mu$is the cationic mobility, E_m denotes the migration enthalpy,μ_0 is proportional to the jump attempt frequency, and k and T are the Boltzmann constant and temperature in K. The frequency f_p derived from ω_{max} is an effective averaged hopping frequency of an ion. The effective pre-factor $f_0$depends on the defect charge carrier density, C.

The process of ion migration through the sample involves the activation energy for migration of ions across the grain boundaries, E_{a2} (obtained from the semicircle corresponding to high frequency) and that for migration of ions within grain (intra-grain) ion migration, E_{a1} (obtained from the semicircle corresponding to low frequency). Evidently, the partial replacement of the host Ag^+ by dopant cations within the grain alters the local environment leaving the grain boundary undisturbed. This alteration in the local environment modifies the activation enthalpy for intra-grain ion migration, whereas that for inter-grain conduction remains invariant.

In the complex impedance plot real and imaginary impedance has been plotted as a parametric function of frequency.

Table 4: Impedance data for (1-*x*) Ag_2SO_4: (*x*) $LiNbO_3$ for x=0, 10, 20, 30, 40, 50, 60 at 235°C(*a*) low frequency semicircle (*b*) high frequency semicircle

From low frequency semicircle

x=	R_{b1}(kΩ)	α_1	f_{p1}	ln(f_{p1})	E_{a1}
0	6981	0.92	2638	12.142	0.61
10	7404	0.77	2238	13.996	0.685
20	5623	0.73	1412	12.279	0.687
30	1731	0.74	1850	11.982	0.647
40	737	0.75	3584	11.283	0.545
50	817	0.73	3162	10.821	0.503
60	733	0.75	2818	10.24	0.45

From high frequency semicircle

x=	R_{b2}(kΩ)	α_2	f_{p2}	ln(f_{p2})	E_{a2}
0	7241	0.87	3327	11.68	0.55
10	7149	0.85	1995	12.158`	0.645
20	4715	0.85	1778	12.634	0.713
30	12108	0.83	446	12.621	0.687

40	14747	0.85	281	11.486	0.55
50	-	-	-	-	-
60	-	-	-	-	-

The bulk resistance, peak frequency, depression of semicircle in complex impedance plot due to intergrain and intragrain ion migration process are presented in **Table 4**.

The variation in activation energies E_{a1} and E_{a2} arising from intergrain and intragrain processes are plotted as a function of $LiNbO_3$ concentration are depicted in **Fig.4**. Around 20-30 wt% concentration offers minimal activation enthalpy for ion migration.

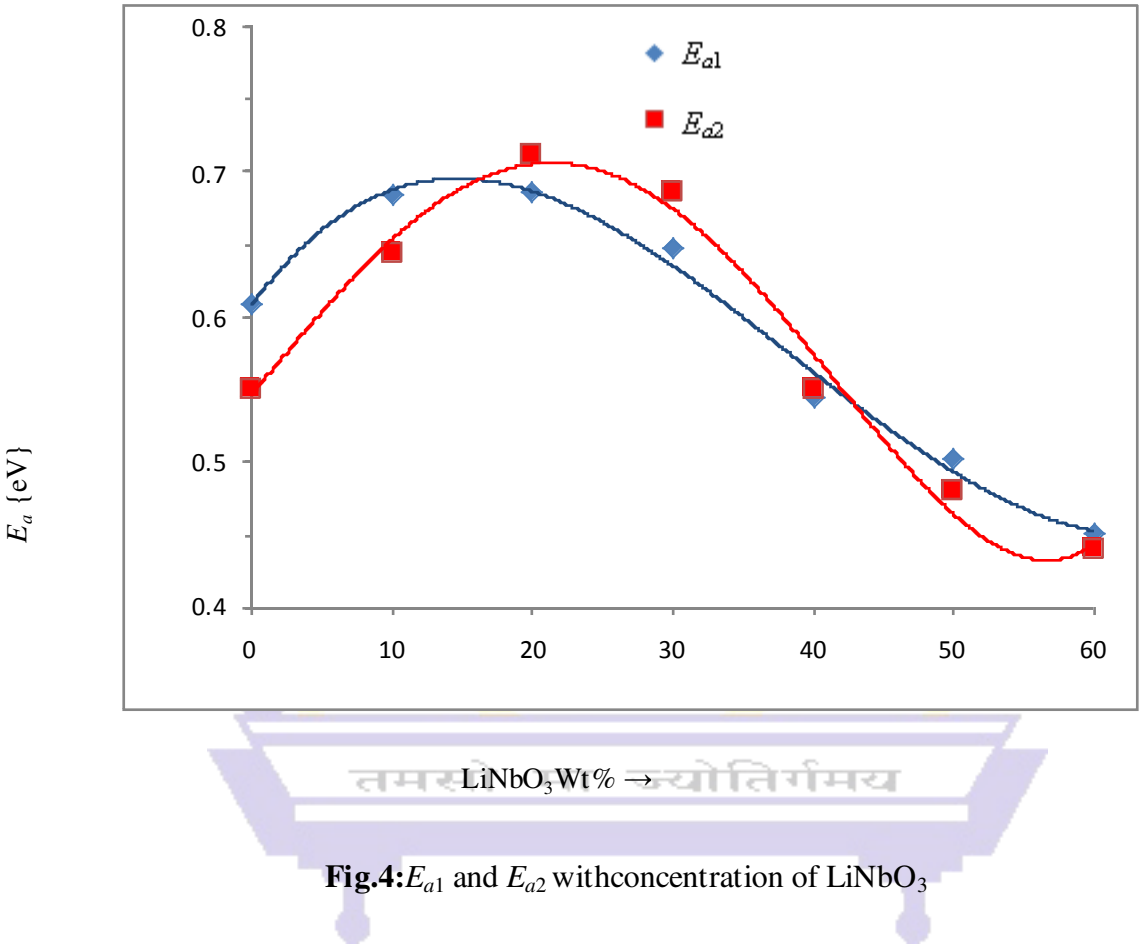

Fig.4: E_{a1} and E_{a2} withconcentration of $LiNbO_3$

Ionic conductivity

The generalized perception of Arrhenius theory of the temperature effect on the reaction rate (ion diffusion) originated from the temperature effect on the equilibrium constant. It is known that:

$$\frac{dln(K)}{d\frac{1}{T}} = -\frac{H}{R} \qquad \ldots(7)$$

where$K$ is an equilibrium constant, R is the gas constant, and H is the heat of reaction. The equilibrium constant is $\frac{k_1}{k_2}$, where k_1 and $k_1$are the rate constants for the forward and reverse reactions respectively. Thus, we obtain;

$$\frac{dln(k_1)}{d\frac{1}{T}} - \frac{dln(k_2)}{d\frac{1}{T}} = -\frac{H}{R} \qquad \ldots(8)$$

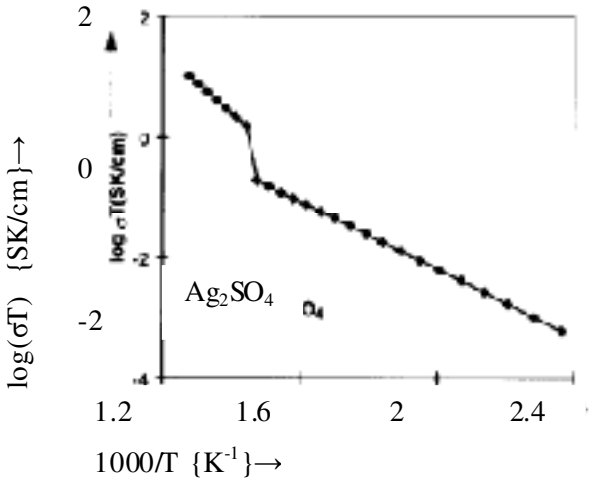

Fig.5: Arrhenius plot for pure Ag_2SO_4 in α and $\boldsymbol{\beta}$ phases

Arrhenius recognized that the last equation could be conveniently divided into two parts, each having the form of:

$$\frac{dln(k)}{d\frac{1}{T}} = -\frac{E}{R} \qquad \ldots(9)$$

Where E is referred by Arrhenius as representing the energy difference between the reactants and an activated species. The term E is, therefore, called the activation energy. Taking E as a constant the last can be integrated to yield:

$$ln(k) = ln(A) - \frac{E}{RT}$$

where$ln(A)$ is the constant of integration and the last equation can be converted to:

$$k = Ae^{-\frac{E}{RT}} \qquad \ldots(10)$$

This form of equation (10) is the most widely adopted form of the Arrhenius equation. The temperature dependent ionic conductivity in all specimens is governed by Arrhenius equation can be expressed as equation (11);

$$(\sigma T) = (\sigma T)_o exp\left(\frac{E_a}{2KT}\right) \qquad \ldots(11)$$

The pre-exponential factor $(\sigma T)_o$ in the above equation (which is appearing out of constant of integration) is related to the frequency of ionic collisions in the collision theory and to the entropy term in the transition state theory. The equation governs forward and reverse reaction contributing to ionic conductivity (σT) and predomination of each other. Arrhenius plots for all the compositions are found to obey the Arrhenius law (11) in both the α and β phases (as an example, **Fig. 5** depicts this behaviour for the host Ag_2SO_4).

The observed change in slope at 416°C with an order of magnitude jump in conductivity in the case of pure Ag_2SO_4 accounts for the orthorhombic β to hexagonal α phase transition (**Fig. 5**). The magnitudes of the conductivities (2.22×10^{-5} S/cm at 250°C and 3.4×10^{-3} S/cm at 440°C) and the transition temperature (416°C) are in close agreement with earlier reports [**xxxviii,xxxix,xl,xli**].

Table 5: Conductivity data in orthorhombic Phase at 250°C

Composition	log(σ)	log(σT)$_o$	E_a
x=0	-4.750	3.457	0.569
x=10	-3.641	4.478	0.560
x=20	-2.988	4.825	0.528
x=30	-2.740	4.898	0.510
x=40	-2.857	5.166	0.550
x=50	-4.033	4.048	0.556
x=60	-4.194	3.926	0.56

Table 5 presents the conductivity σ, pre-exponential factor (σT)$_o$, activation enthalpy for ion migration E_a for entire series of the samples under study in low temperature orthorhombic phase.

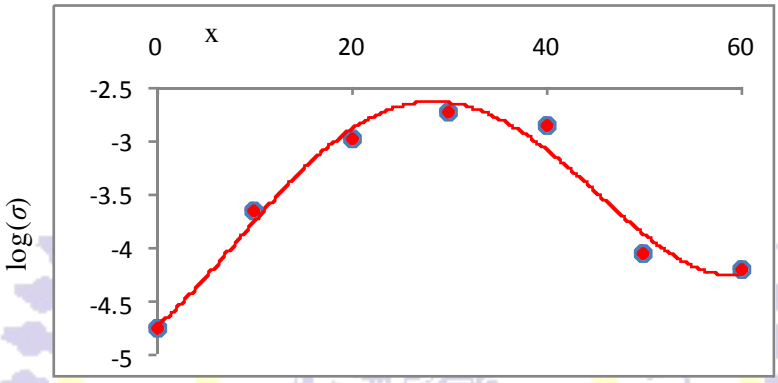

Fig.6: Concentration dependent conductivity at 250°C

The concentration dependent trend in **Fig. 6**suggests that the composite solid electrolyte offers highest conductivity at x=30 wt%. Moreover, the activation energy required in process of ion migration offers minima for 30 wt% dispersed $LiNbO_3$ in Ag_2SO_4. **Fig.7** depicts the concentration dependent variation of activation energy.

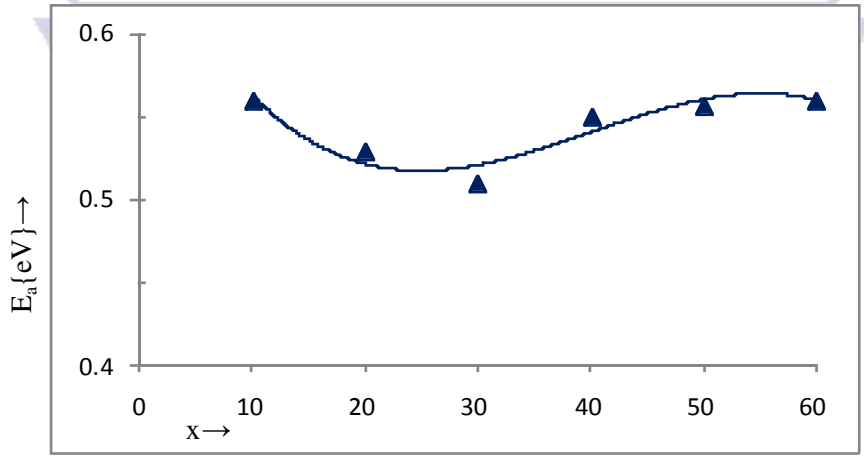

Fig.7: Concentration dependent activation enthalpy for ion migration

When the conductivity data is fit in Arrhenius equation (**11**), the pre-exponential factor arising out of line fitting offers a critical value at x=30wt% as shown in **Fig.8**.

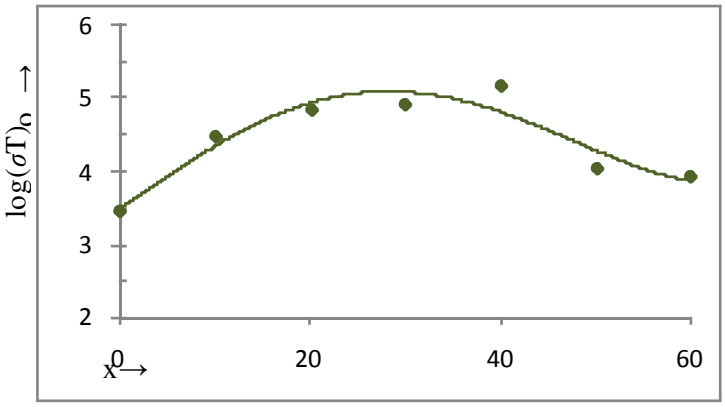

Fig.8: Concentration dependent pre-exponential factor

Conclusion:

Interfaces allow a variety of optimization strategies for materials. Boundary effects on transport phenomena are of outstanding importance in ionic conductor composites: given their anisotropy, interfaces can act as transport pathways or transport barriers (core effect) and they can affect the charge carrier distribution in adjacent regions, due to defect segregation at the interface (space charge effect).

Given the reduced interface core area in conventional composites, the space charge effect is often more important for practical properties. The conductivity enhancement observed in ceramic composite materials can be at-least qualitatively understood and in some cases even quantitatively described by simple analytical equations derived from space charge theory. Many other experimental observations are also consistent with the "abrupt core-space charge model". However, more complicated situations can be encountered, for example when structural perturbations near interface sextent over a larger range, including presence of dislocations or meta-stable phases. Space charge effects at interfaces between nano-crystalline inclusions and a glass matrix can also explain the conductivity enhancement in some glass-ceramic composites.

Apart from the need for solid electrolytes with suitable mechanical properties, ionic conductivity may be improved by better knowledge of the interface properties, including studies of the possibility of space charge effects in the ceramic-polymer boundary region in dense composites.

The material 70 Ag_2SO_4:30 $LiNbO_3$ offers better electrical properties in terms of higher ionic conductivity low activation enthalpy of ion migration as compared to pure Ag_2SO_4 without alteration in ionic transference number. These results are consistent[**xlii**,[xliii]] with the similar system when $BaTiO_3$ is dispersed in Ag_2SO_4. This material may have higher potential for application as silver ion conducting solid electrolyte in batteries and sensors as offers improved electrical and mechanical properties.

Refrences :

[1].Kro Èger, F.A. The Chemistry of Imperfect Solids 2nd Ed **1974**.

DOI:http://www.worldcat.org/title/chemistry-of-imperfect-crystals-2-imperfection-chemistry-of-crystalline-solids/oclc/490295263

[2]. Maier J. Prog. Solid St. Chem. **1995** 23, 171.

DOI:10.1016/0079-6786(95)00004-E
[3.] Liang C.C. J. Electrochem. Soc.**1973** 120, 1289.
DOI: 10.1149/1.2403248
[4.] Padma Kumar, P.; Yashonath, S. J. Chem. Sci.**2006** 118(1) 135
DOI::10.1007/BF02708775
[5.]Torrie,G. M.; Valleau, J. P. J. Phys. Chem., **1982**, 86 (16), 3251.
DOI: 10.1021/j100213a035
[6.]Verwey, J.W.; J.Th.G. Overbeek, Theory of the Stability of Lyophobic Colloids**1948** (Elsevier, New York).
DOI: 10.1002/pol.1949.120040321
[7.]Lehovec K. J. Chem. Phys.**1953** 21, 1123.
DOI: http://dx.doi.org/10.1063/1.1699148
[8.]Wagner C. J. Phys. Chem. Solids**1972** 33, 1051.
DOI:http://dx.doi.org/10.1016/S0022-3697(72)80265-8,
[9.]Jow, T.; Wagner, J.B. J. Electrochem.Soc.**1979** 126, 1963.
DOI:10.1149/1.2128835
[10.]Maier, J. J. Phys. Chem. Solids**1985** 46, 309.
DOI:10.1016/0022-3697(85)90172-6,
[11.] Maier, J. Nature Materials 4, 805 - 815 (2005)
DOI:10.1038/nmat1513
[12]Agrawal, R.C.; Gupta, R.K. J. Mater.Sci.**1999** 34, 1131.
DOI: 10.1023/A:1004598902146
[13.]Gauthier. M: Chamberland, A. J. Electrochem.Soc.**1977** 124, 1579.
DOI:10.1149/1.2133114
[14.]Ramaswamy, V; Vimalathithan, R M; Ponnusamy, V Adv. Mat. Lett.**2012**, 3(1), 29-33
DOI: 10.5185/amlett.2011.4240
[15.]Liu, H Y; Hupp, J T; Weave, M J J. of ElectroanalChemy& Interfacial Electrochem**1984** 179, 1-2, 219.
DOI: 10.1016/S0022-0728(84)80290-9
[16]Liu, S H; Hinnen, C; Huong, C; Tacconi, N R; Hoa, K M; J of ElectroanalyticalChem& Interfacial Electrochem**1984** 176, 1–2, 325.
DOI: doi:10.1016/S0022-0728(84)80327-7
[17.] Mari, C.M.; Beghi, M; Pizrini, S. Sensors and Actuators B, **1990**, 2, 51-55.
DOI: 10.1016/0925-4005(90)80008-N
[18.]Singh, K; Anwane, S W; Bhoga, S S Solid State Ionics**1996** 86-87, 187.
DOI: 10.1016/0167-2738(96)00120-8
[19.]Singh, K; Pande, S M; Anwane, S W; Bhoga, S S App. Phy.A**1998** 66, 205.
DOI: 10.1007/s003390050657
[20.]Singh, K; Pande, S M; Bhoga, S S Bull Mater Sci**1995** 19(3) 237.
DOI: http://www.ias.ac.in/jarch/bms/18/00000246.pdf
[21]Anwane, S W; Anwane, R S Adv. Mat. Lett.**2012**, 3(2), 77.

DOI: 10.5185/amlett.2012.1314
[22.] Anwane, S W Adv. Mat. Lett.**2012**, 3(3), 204.
DOI: 10.5185/amlett.2012.4332
[23.] Singh K; Pande S M; Anwane S W; Bhoga S S Bull.of Electrochem**1996** 12 (11-12) 625.
DOI: 10.1007/BF02745557
[24.] Atkinson, A. Solid State Ionics**1988** 28±30, 1377.
DOI:http://dx.doi.org/10.1016/0167-2738(88)90390-6,
[25.] Wuensch, B.J.; Tuller, H.L. J. Phys. Chem. Sol.**1994** 55, 975.
DOI:http://dx.doi.org/10.1016/0022-3697(94)90117-1
[26.] Aoki, M.; Chiang, Y.M.; Kosacki, I.; Lee, J.R.; Tuller, H.L.; Liu, Y. J. Am. Ceram. Soc.**1996** 79, 1169.
DOI: 10.1111/j.1151-2916.1996.tb08569.x
[27.] Ikeda, J.A.S.; Chiang, Y.M. J. Am. Ceram.Soc.**1993** 76, 2437 and 2447.
DOI: 10.1111/j.1151-2916.1993.tb03964.x
[28.] Blom, D.A.; Chiang, Y.M. Mat. Res. Soc. Symp. Proc.**1997** 458, 127 (Materials Research Society, 1997).
DOI:
[29] Yeh, N C; Fu, C C; Wei, J Y T; Vasquez, R P; Huynh, J; Maurer, S M; Beach, G; Beam, D A J. Appl. Phys.**1997** 81, 8,5499.
DOI: 10.1063/1.364580
[30.] Jin, S; Tiefel, T H; McCormack, M; Fastnacht, R A; Ramesh, R; Chen, L H Appl. Phys. Lett.**1995** 66, 382.
DOI: 10.1063/1.114220
[31.] Hwang, H Y; Cheong, S W; Radaelli, P G; Marezio, M; Batlogg, B Phys. Rev. Lett.**1995** 75, 914.
DOI: 10.1103/PhysRevLett.75.914
[32.] Moritomo, Y; Asamitsa, A; Tokura, Y; Phys.Rev.B**1995** 51, 16 491.
DOI: 10.1103/PhysRevB.51.16491
[33.] Khazeni, K; Jia, Y X; Lu, L; Crespi, V H; Cohen, M L; Zettl, A Phys. Rev. Lett.**1996** 76, 2, 295.
DOI: 10.1103/PhysRevLett.76.295
[34.] Ibarra, M R; Algarabel, P A; Marquina, C; Blasco, J; Garcia, J; Phys. Rev. Lett.**1995** 75, 3541.
DOI: 10.1103/PhysRevLett.75.3541
[35.] Zhao, G M; Conder, K; Keller, H; Muller, K A Nature**1996** 381, 676.
DOI: 10.1038/381676a0
[36.] Singh, K Solid State Ionics**1993** 66, 5.
DOI:10.1016/0167-2738(93)90021-T
[37.] Muccilloa, ENS; Kleitzb, M Journal of the European Ceramic Society**1996** 16(4) 453.
DOI:10.1016/0955-2219(95)00125-5
[38.] Liu, Q; Worrel, W L Solid State Ionics**1988** 28-30(2) 1668.
DOI: 10.1016/0167-2738(88)90439-0
[39.] Weppner, W Solid State Ionics**1981** 3(4) 1.
DOI:10.1016/0167-2738(81)90044-8 12
[40.] Weppner, W Solid State Ionics**1981** 5 (3).
DOI: 10.1016/0167-2738(81)90186-7 13
[41.] Weppner, W Sens& Actu**1987** 12(2) 107.
DOI: 10.1016/0250-6874(87)85010-2

[42.] Anwane S W Adv. Mat. Lett.**2013**, 4(4) Page- 300-309
DOI:10.5185/amlett.2012.8404
[43.] Anwane, S W Adv.Mat.Lett. 2013 (Inpress).